Journal of Environmental Radioactivity 182 (2018) 117–127

Contents lists available at ScienceDirect

Journal of Environmental Radioactivity

journal homepage: www.elsevier.com/locate/jenvrad

Time resolution requirements for civilian radioxenon emission data for the CTBT verification regime

Pieter De Meutter[a,b,c,*], Johan Camps[a], Andy Delcloo[b], Benoît Deconninck[d], Piet Termonia[b,c]

[a] Belgian Nuclear Research Institute, Boeretang 200, 2400 Mol, Belgium
[b] Royal Meteorological Institute of Belgium, Ringlaan 3, 1180 Brussels, Belgium
[c] Department of Physics and Astronomy, Ghent University, Krijgslaan 281, 9000 Gent, Belgium
[d] Institute for RadioElements, Avenue de l'Espérance 1, 6220 Fleurus, Belgium

ARTICLE INFO

Keywords:
ATM
CTBT
Medical isotope production facilities
Radioxenon monitoring

ABSTRACT

The capability of the noble gas component of the International Monitoring System as a verification tool for the Comprehensive Nuclear-Test-Ban Treaty is deteriorated by a background of radioxenon emitted by civilian sources. One of the possible approaches to deal with this issue, is to simulate the daily radioxenon concentrations from these civilian sources at noble gas stations by using atmospheric transport models. In order to accurately quantify the contribution from these civilian sources, knowledge on the releases is required. However, such data are often not available and furthermore it is not clear what temporal resolution such data should have. In this paper, we assess which temporal resolution is required to best model the ^{133}Xe contribution from civilian sources at noble gas stations in an operational context. We consider different sampling times of the noble gas stations and discriminate between nearby and distant sources. We find that for atmospheric transport and dispersion problems on a scale of 1000 km or more, emission data with subdaily temporal resolution is generally not necessary. However, when the source-receptor distance decreases, time-resolved emission data become more important. The required temporal resolution of emission data thus depends on the transport scale of the problem. In the context of the Comprehensive Nuclear-Test-Ban Treaty, where forty noble gas stations will monitor the whole globe, daily emission data are generally sufficient, but for certain meteorological conditions, better temporally resolved emission data are required.

1. Introduction

Certain radioactive xenon isotopes (^{131m}Xe, ^{133m}Xe, ^{133}Xe and ^{135}Xe with half-lives of respectively 11.84 d, 2.20 d, 5.25 d and 9.14 h) are monitored globally as part of the International Monitoring System (IMS) with the purpose of verifying compliance with the Comprehensive Nuclear-Test-Ban Treaty. Once the Treaty will enter into force, forty IMS stations will monitor these noble gases, with the option to increase the number of stations to eighty. To date, thirty IMS noble gas stations have been installed. Atmospheric transport modelling can be used to help determine the origin of suspicious detections made by the IMS noble gas network.

The IMS noble gas stations sample high volumes of air during a period of 12 h or 24 h (depending on the detection system), during which xenon is extracted from the air (see for instance Ringbom et al., 2003; Fontaine et al., 2004). These noble gas detection systems are still being improved: in the future, systems will collect more xenon during a shorter sampling period, allowing a better source localisation in case of a suspicious detection. For instance, the sampling time of the SAUNA III system will be reduced to 6 h instead of 12 h (Ringbom et al., 2017), the sampling time of the SPALAX-New Generation system will be reduced to 8 h instead of 24 h (Topin et al., 2017) and the sampling time of Xenon International will be 6 h (Hayes et al., 2015).

However, the capability of the IMS noble gas network to pick up radioxenon signatures from a nuclear explosion is deteriorated by civilian sources that also emit radioxenon. These civilian sources are mainly medical isotope production facilities (Saey, 2009; Kalinowski et al., 2014) and nuclear power plants (Appelhans and Turnbull, 1981; Kalinowski and Pistner, 2006). Their effect on the IMS noble gas network has been addressed in several studies (Hoffman et al., 2009; Wotawa et al., 2010; Achim et al., 2016; Gueibe et al., 2017).

One of the approaches to deal with this issue, is to simulate the daily radioxenon concentrations from civilian sources at IMS stations by using atmospheric transport models (for instance, Schöppner et al., 2013; Eslinger et al., 2016; De Meutter et al., 2016; Maurer et al., 2017). In principle, this allows to check whether a detection at an IMS

* Corresponding author. Belgian Nuclear Research Institute, Boeretang 200, 2400 Mol, Belgium.
E-mail address: pieter.de.meutter@sckcen.be (P. De Meutter).

https://doi.org/10.1016/j.jenvrad.2017.11.027
Received 22 September 2017; Received in revised form 21 November 2017; Accepted 22 November 2017

noble gas station is originating from civilian sources instead of a nuclear explosion. However, modelling the daily radioxenon activity concentration is a difficult task and a perfect match between simulated and observed concentrations is not possible due to the turbulent nature of atmospheric dispersion. In order to quantify the contribution from civilian sources to the radioxenon activity concentrations at IMS stations, knowledge on the releases from civilian sources is required. However, such data are often not available due to their commercial value. Furthermore, it is not known which temporal resolution such emission data should have to best model the radioxenon activity concentration. Schöppner et al. (2013) used an atmospheric transport model and different emission data sets with daily, weekly, monthly and yearly time resolution to model the ^{133}Xe concentration at two IMS stations from the medical isotope production facility Ansto near Sidney, Australia. They found an improvement for the nearest IMS station (700 km from Ansto) when using daily emission data. No clear improvement was observed for the station at 3000 km from Ansto. Schöppner et al. (2014) found that monthly emission data from the Institute for Radio-Elements in Fleurus (Belgium) had no benefit over yearly emission data for an IMS station in Schauinsland (Germany; the source-receptor distance was approximately 380 km), suggesting that emission data with a higher temporal resolution is necessary to better model the ^{133}Xe concentration. (Eslinger et al., 2016) presented an intercomparison study of the modelled radioxenon concentration for the same source and station, and found that models using 15-min emission data had higher ranks than models using longer release periods. However, models using 3-hourly release periods had higher ranks than models using 1-hourly release periods. These models differed not only by their release period, so that other effects might have played a role.

In recent years, efforts were undertaken to bring together the radioxenon monitoring community with the medical isotope production community through a series of workshops (Matthews et al., 2012; WOSMIP, 2016). Awareness on the civilian radioxenon background is being created and emission data are shared for scientific research in an ad-hoc way. Verification activities conducted under the Comprehensive Nuclear-Test-Ban Treaty could benefit from having available emission data for modelling the radioxenon civilian background.

In this paper, we assess which temporal resolution is required for civilian ^{133}Xe emission data to model the ^{133}Xe background in an operational context. We consider different IMS station sampling periods (12 h for the current SAUNA systems, 24 h for the current SPALAX systems and, anticipating the installation of improved noble gas detection systems, 6 h). Furthermore, we also consider different source-receptor distances.

The paper is structured as follows. Section 2 describes the method and the Lagrangian particle dispersion model Flexpart used in this study. Section 3 describes the findings on the temporal resolution requirements of emission data for operational atmospheric transport and dispersion modelling. A discrimination based on the source-receptor distance is made. The effect of the sampling period (24 h, 12 h or 6 h) is addressed in section 4. Section 5 illustrates the findings from previous sections by considering emission data from the medical isotope production facility Institute of Radio-Elements with the highest available temporal resolution (emission data are available every 15 min). The effect of the spatial resolution is briefly assessed in section 6. A discussion and conclusions are given in section 7.

2. Method

2.1. Atmospheric transport and dispersion simulations

The Lagrangian particle dispersion model Flexpart has been used for the atmospheric transport and dispersion simulations (Stohl et al., 2005; Stohl and Thomson, 1999). Flexpart takes into account advection by the mean wind, mesoscale and turbulent wind fluctuations, and, if applicable, dry and wet deposition and radioactive decay. Furthermore, convection can be taken into account (Seibert et al., 2001) via the scheme of Emanuel and Živković-Rothman (1999). Diffusivity in the atmospheric boundary layer is parameterised via the Hanna scheme (Hanna et al., 1982). The height of the atmospheric boundary layer is determined by Flexpart via the critical Richardson number (Vogelezang and Holtslag, 1996). Flexpart has been validated with data from large-scale tracer experiments (Stohl et al., 1998).

2.2. Experimental set-up

Flexpart was run with numerical weather data from the IFS or Integrated Forecasting System of the European Centre for Medium-Range Weather Forecasts (ECMWF) extracted from the MARS archive. Four analyses per day at times 00, 06, 12 and 18 UTC were combined with forecasts at 3 h lead time (00 + 03 h, 06 + 03 h, 12 + 3 h and 18 + 03 h), so that meteorological data were available every three hours. Software available at the Flexpart website (www.flexpart.eu) has been used for the extraction of the meteorological data. The extracted meteorological data had 1° horizontal grid spacings and 137 non-uniform vertical levels.

We considered two IMS noble gas stations in the northern hemisphere: station RN63 in Stockholm, Sweden, and station RN22 in Guangzhou, China. The former station, located at 59.4° N, is hypothesised to be representative for stations in the mid-latitudes, while the latter, located at 23.1° N, is hypothesised to be representative for stations in the tropics.

The atmospheric transport and dispersion simulations were run in backward mode (Seibert and Frank, 2004), so that virtual ^{133}Xe particles were released from the two IMS stations considered in this study and were dispersed over the domain backwards in time during a period of thirty days. A total of 1,000,000 particles were released in every simulation. Simulations were started every six hours for a winter period (15th of December 2015 until the 15th of March 2016, further on called DJF (Dec - Jan - Feb); the first simulation finished on the 15th of November 2015) and a summer period (16th of June until the 15th of September, further on called JJA (Jun - Jul - Aug); the first simulation finished on the 16th of May 2016) for both stations. Each simulation consisted of a 6 h release, which is representative for an IMS station sampling time of 6 h. The result are so called source-receptor-sensitivities, which were stored every hour. Here, the source-receptor-sensitivities have units of time and can be interpreted as a particle residence time (Seibert and Frank, 2004). By averaging the source-receptor-sensitivity fields from consecutive simulations, we can mimic an IMS station sampling time of 12 h or 24 h without the need for additional simulations. Radioactive decay was taken into account during runtime.

We assumed that both release and detection take place in the lowest model layer of Flexpart, which was set from surface level to 100 m above surface (note that during the simulations, the top of the atmospheric transport model domain was the same as the top of the meteorological model, which was 0.01 hPa). The horizontal dimensions of a grid box were, as for the meteorological data, 1°.

2.3. Quantifying the source-receptor-sensitivity time fluctuation

The source-receptor-sensitivity (SRS) matrix $\mathbf{M}$ relates an observation vector $\mathbf{y}$ with a source vector $\mathbf{x}$ via the relation:

$$\mathbf{y} = \mathbf{M}\mathbf{x} \quad (1)$$

Note that the source-receptor-sensitivity matrix $\mathbf{M}$ is also known as the transfer coefficient matrix (see for instance Draxler and Rolph, 2012).

We consider the relevant radioxenon sources as grid box sources. Consider the source-receptor-sensitivity relation between a time-dependent grid box source $x(x_s, y_s, z_s; t)$ located in grid box (x_s, y_s, z_s) and

an IMS station observation $y(x_0, y_0, z_0, t_{start}, t_{stop})$ taken at location (x_0, y_0, z_0) and between sampling times t_{start} and t_{stop}; Eq. (1) can now be written as a sum over the grid box sources (index s) and times (index t):

$$y_i(x_0, y_0, z_0, t_{start}, t_{stop}) = \sum_s \sum_t M(x_0, y_0, z_0, t_{start}, t_{stop}, x_s, y_s, z_s; t)\, x(x_s, y_s, z_s; t) \quad (2)$$

For ease of notation, we now write $m_t \equiv M(...;t)$. From Eq. (2), we see that the temporal resolution of the source term x that allows to best model an observation y_i should equal the temporal resolution of the source-receptor-sensitivity M. If the source term x would have a higher temporal resolution, that would not add extra information since the summation over time will average out the higher temporal resolution. Indeed, assume that m_t can be approximated by its average $\overline{m}$ during a certain (sufficiently small) time interval; in that case, only the accumulated release $\sum_t x(t)$ is "seen" by the model and the details of the release of $x(t)$ do not influence the model output:

$$\sum_t m_t\, x(t) \approx \overline{m} \sum_t x(t) \quad (3)$$

Consider a time series of SRS values $m_{t_0}, m_{t_1}, ..., m_{t_N}$. Our goal is to assess how the SRS values change with time, in order to give recommendations on which temporal resolution emission data should best have. For that, we quantify how a value m_t relates to $m_{t+\tau}$ for a chosen time lag τ: we calculate (i) the autocorrelation and (ii) the fraction $m_t/m_{t+\tau}$ for different time lags τ (we take the inverse in case the fraction is smaller than 1, since we are not interested in which of both values is largest). This SRS fraction, when plotted on a logarithmic axis, can be seen as the difference between the logarithm of the SRS values, which is motivated by the fact that the SRS values span many orders of magnitude.

The autocorrelation for a certain time lag τ is defined as:

$$autocorrelation(\tau) = \frac{E[m_t - \overline{m}]\, E[m_{t+\tau} - \overline{m}]}{\sigma^2} \quad (4)$$

were m_t is the SRS at time t, $\overline{m}$ is the mean SRS value, $E[...]$ is the expectation value and σ^2 the variance of the SRS. It measures the correlation of the SRS value m_t at time t with the SRS value $m_{t+\tau}$ for a certain time lag τ. It is expected that the autocorrelation is close to one for small time lags, and goes to zero for larger time lags. When the autocorrelation reaches zero for a certain time lag, there is no correlation any more between the SRS values m_t and $m_{t+\tau}$.

For the calculation of the SRS fraction m_{t_k}/m_{t_l}, we first apply an SRS threshold to exclude small SRS values that would create large ratios. Applying such a threshold is further justified by the fact that very small SRS values have a negligible impact on the activity concentration at the receptor. We use the longest series of consecutive SRS values above the threshold for each Flexpart simulation.

The SRS threshold is set to 0.1 s, since SRS values below that threshold hardly contribute to the observed concentration y in Eq. (2). Indeed, an SRS of 0.1 s and a source of 10^{12} Bq/h (which is roughly equal to the maximum release of 10^{13} Bq/day for civilian sources (Saey, 2009)), results in a contribution to the activity concentration of 0.0014 mBq/m^3 (for comparison, the minimum detectable concentration is of the order of 0.1 mBq/m^3; the volume of the grid boxes is not constant for the lat-lon grid that has been used, therefore, the median value of the grid box volume has been used).

2.4. Selection of fictitious sources

Flexpart outputs a three-dimensional source-receptor-sensitivity field at every simulation hour. Three grid boxes in the lowest model level have been selected at distances between 250 and 350 km, 950–1050 km and 5000–6000 km for each set of simulations with a fixed IMS station and period (Fig. 1). These grid boxes represent fictitious sources. The selection is based on the number of times that the SRS value exceeded the chosen threshold, to ensure that the selected points have the best available statistics.

During the winter period, air masses near station RN63 were coming from a large region (Fig. 1a). An important feature determining the circulation towards station RN63 in winter is the Siberian high (see for instance Panagiotopoulos et al., 2005), which creates a southeasterly flow towards station RN63. The nearby fictitious sources are located west and southeast from the station. The remote fictitious source is located in Canada. During the summer period, a south-westerly flow prevails and all three fictitious sources are situated south-west of the station (Fig. 1b).

As for station RN63, station RN22 exhibits two circulation regimes depending on the season. In winter, air masses near station RN22 are coming from the north (Fig. 1c), while in summer, air masses are originating from the southwest (Fig. 1d). Thess features correspond with the East-Asian monsoon (see for instance Wu and Wang, 2002; Chang, 2004).

3. Source-receptor-sensitivity temporal variation

As described in the previous section, the temporal variation of the SRS time series is assessed by taking the ratio of SRS pairs separated by a certain time lag, and by calculating the SRS autocorrelation. In this section, a 24 h sampling period for the IMS noble gas stations is assumed, which was obtained by averaging the output of four consecutive Flexpart simulations (the effect of shorter sampling periods will be discussed in the next section). Results are shown for three different source-receptor distances of approximately 300 km, 1000 km and 5000 km (the selection of these sources was described in the previous section).

3.1. SRS fractions

Fig. 2 shows the SRS fractions for the two IMS stations (RN63 and RN22) and periods (DJF, JJA) considered in this study. Three features can be seen: (i) not surprisingly, the SRS fraction grows for larger time lags in a roughly asymptotic way. There is a steep increase in SRS fractions during the first 6 h, and afterwards a slow increase or even no increase. (ii) The SRS fractions do not show a consistent regional (RN22 versus RN63) or seasonal dependency (DJF versus JJA). There is quite some spread between different IMS stations and periods, especially for the 0.95 quantile of the SRS fraction, but these differences are not consistent among the different source-receptor distances. (iii) The source-receptor distance has a clear impact on the SRS fractions: smaller fractions are found for larger source-receptor distances.

For the smallest source-receptor distance (Fig. 2a), the median SRS fractions steadily grow to a value between 3 and 4 for a time lag of 24. The 0.95 quantile of the SRS fraction quickly becomes very large, with values ranging between 10 and 50 for a time lag of only 6 h. At a time lag of 24 h, the values range between 20 and 100. For the intermediate source-receptor distance (Fig. 2b), the median SRS fractions reach a value around 2 at a time lag of 24 h. The 0.95 quantile ranges between 5 and 10 at a 6 h time lag, and between 10 and 20 at a 24 h time lag. For the largest source-receptor distance (Fig. 2c), the median SRS fractions are only slightly lower than those at intermediate source-receptor distance. The 0.95 quantile is significantly smaller and does not exceed a value of 5.

We conclude that for atmospheric transport and dispersion problems on the synoptic scale (having spatial scales of 1000 km and more; Fig. 2b and c), SRS values above the chosen threshold generally do not vary much within 24 h. Therefore, daily emission data are sufficient for these cases. For smaller source-receptor distances, the 0.95 quantile of the SRS fractions reach 50 after only a few hours and 100 after 24 h. For these cases, related to specific atmospheric conditions that can be identified by the atmospheric transport model, emission data with a higher temporal resolution are required.

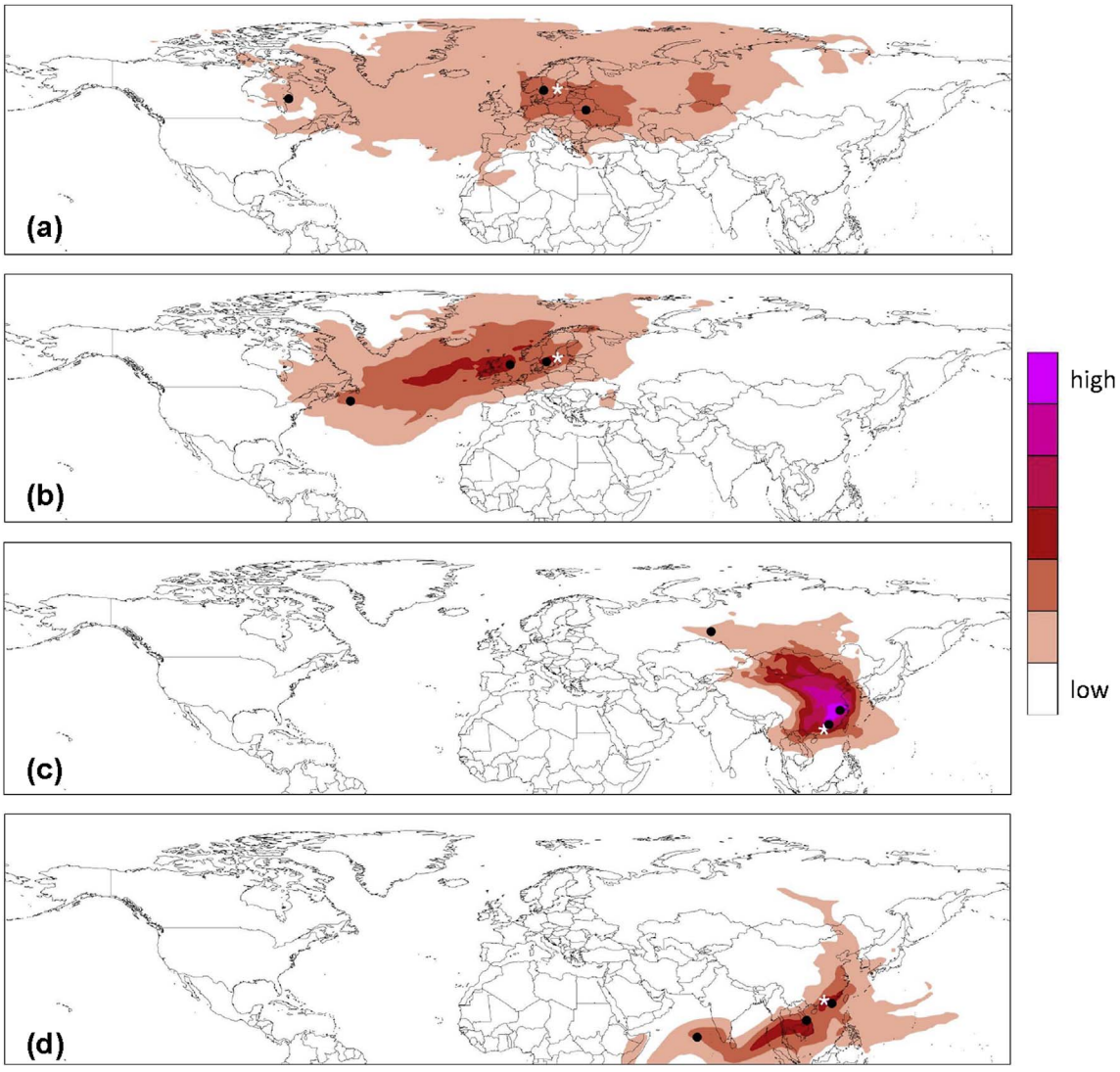

Fig. 1. Selection of fictitious grid box sources based on the number of times that the source-receptor-sensitivity in a certain grid box exceeded a chosen threshold of 0.1 s. From top to bottom: (a) station RN63, winter; (b) station RN63, summer; (c) station RN22, winter; (d) station RN22, summer. For all four sets of simulations, three fictitious sources have been selected (filled circle) within distances of 250–350 km, 950–1050 km and 5000–6000 km from the IMS station (white star).

3.2. SRS autocorrelations

The autocorrelation for each IMS station, each period and each source-receptor distance is shown in Fig. 3. No SRS threshold has been applied here. Three features found in the SRS fractions (Fig. 2) are also found here: (i) the autocorrelation decreases with increasing time lag, (ii) the choice of IMS station or season does not consistently affect the autocorrelation and (iii) the autocorrelation is bigger for larger source-receptor distances.

For the smallest source-receptor distance (Fig. 3a), the median SRS autocorrelations is between 0.4 and 0.6 for a 12 h time lag. At a time lag of 24 h, there is almost no autocorrelation. The 0.05 quantile of the autocorrelation is roughly 0 after a time lag of 6 h. For the intermediate source-receptor distance (Fig. 3b), the SRS autocorrelations are significantly higher than for the smallest source-receptor distance, with a median value up to 0.5 for a 24 h time lag, except for the experiment RN63 JJA. Although some autocorrelation is present at a time lag of 12 h for the 0.05 quantile, there is no correlation at a time lag of 24 h. For the largest source-receptor distance (Fig. 3c), the SRS autocorrelations are even slightly higher, with median values around 0.6 and the 0.05 quantile between 0.1 and 0.3 for a 24 h time lag.

Similar to the discussion on the SRS fractions above, we find that for synoptic scale atmospheric transport and dispersion problems (having source-receptor distances of 1000 km and more), the autocorrelation is generally around 0.5 or more, so that daily emission data is sufficient to model the ^{133}Xe background. However, as above, the 0.05 quantile shows that for certain cases (related to the atmospheric conditions), the autocorrelation drops to zero, suggesting that emission data on shorter time intervals are needed. This is particularly true for short source-receptor distances.

4. Effect of the sampling period on the SRS temporal variation

In this section, we assess the effect of the sampling period of the IMS noble gas detection systems on the temporal resolution of the SRS time series. For that, we consider sampling times of 24 h, 12 h and - anticipating the use of improved detection systems - 6 h. In the Flexpart simulations in backward mode, this corresponds to a release of particles at the receptor with a duration of 24 h, 12 h and 6 h.

Fig. 4 shows the SRS fraction as a function of time lag for different sampling times and source-receptor distances. The results from stations RN22, RN63 and periods DJF and JJA have been combined by taking the median of these four experiments, in order to avoid overburdening the plots with information.

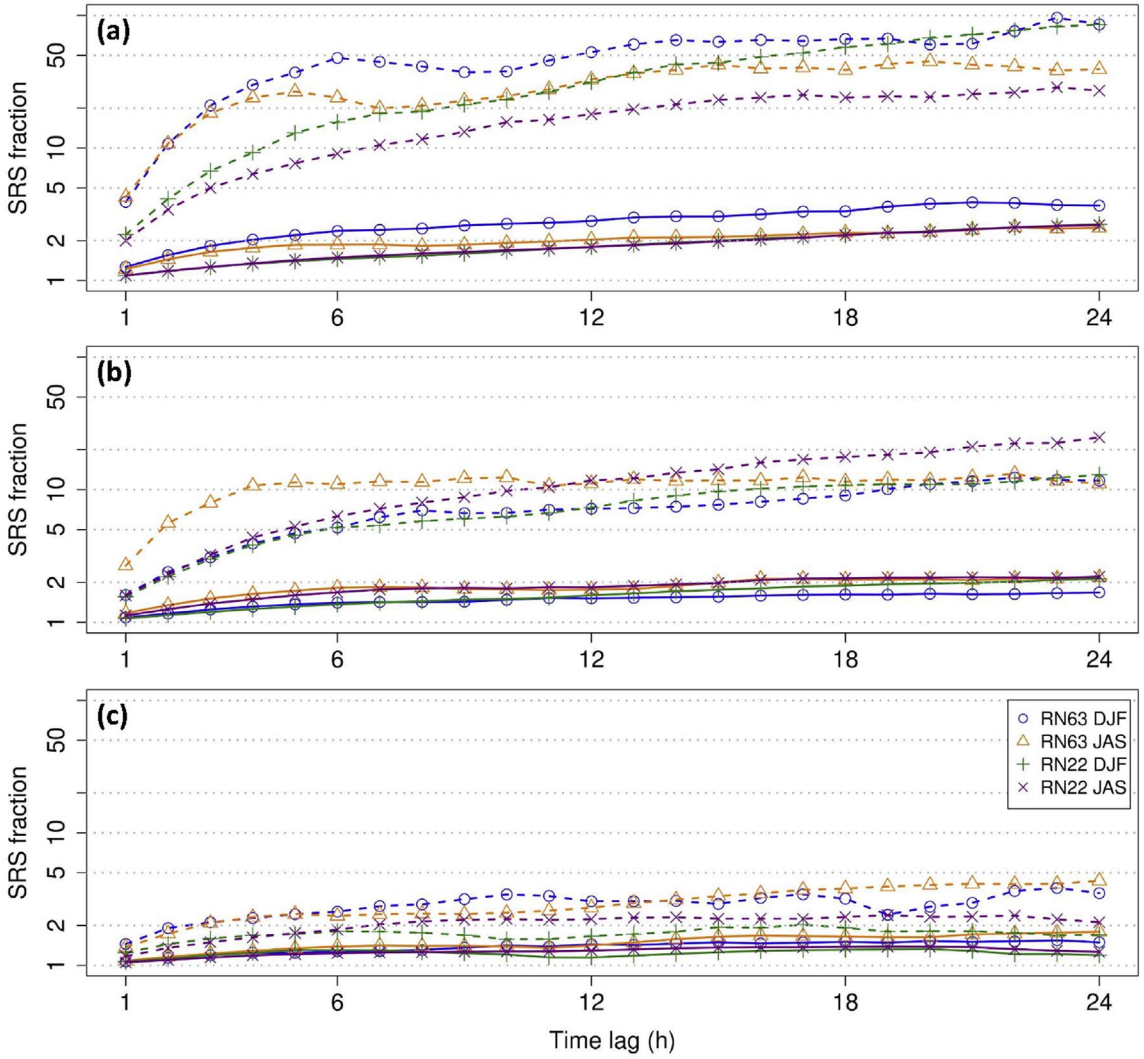

Fig. 2. Median (solid lines) and 0.95 quantile (dashed lines) of the fractions of source-receptor-sensitivity pairs separated by a certain time lag for a source-receptor distance of approx. (a) 300 km, (b) 1000 km and (c) 5000 km. The larger SRS value is always divided by the smaller, so that no values are smaller than 1. Results are given for the two IMS stations and the two periods considered in this study.

For the smallest source-receptor distance (Fig. 4a), the median SRS fractions show a slight dependency on sampling period, with slightly larger fractions for shorter sampling times. The effect of the sampling time on the 0.95 quantile of the SRS fraction is, a priori surprisingly, dependent on the time lag. There is a strong effect between time lags 4 h and 11 h: the simulations with 6 h sampling time have an almost five times larger SRS fraction than the simulations with 24 h sampling time. The reason for this apparent dependency on the time lag is probably that for 6 h sampling time, the SRS fraction reaches its maximum value faster and is thus more quickly saturated. This effect disappears when the runs with 12 h and 24 h sampling time also reach their maximum value (around time lags 14 h and 20 h).

For the intermediate source-receptor distance (Fig. 4b), again slightly larger SRS fractions are found for smaller sampling times, both for the median and 0.95 quantile. Similar to the case with the smallest source-receptor distance, the 0.95 SRS fraction quantile shows an apparent dependency on the time lag, which can again be explained by a different time lag for reaching the saturation SRS fraction, but here the differences are not larger than a factor of three. For a 24 h sampling period, the 0.95 quantile remains roughly a factor of two lower for times lags between 18 and 24 h, while the fractions for a sampling period of 12 h and 6 h converge.

For the largest source-receptor distance (Fig. 4c), the effect of the sampling time seems negligible on the median SRS fractions. The 0.95 quantile slightly increases for shorter sampling times.

Fig. 5 shows the SRS autocorrelation as a function of time lag for different sampling times and source-receptor distances. As above, the results from stations RN22, RN63 and periods DJF and JJA have been combined by taking the median of these four experiments. For all source-receptor distances, the autocorrelation is larger for longer sampling times. The only exception is the 0.05 quantile of the autocorrelation for the smallest source-receptor distance: all three runs become quickly uncorrelated.

The results from this section suggest that, from the viewpoint of atmospheric transport modelling, the added value of having more observations due to shorter sampling times is accompanied by the disadvantage that somewhat larger errors can occur while trying to predict the ^{133}Xe background from civilian sources when detailed emission data are not known.

5. Example using real stack monitoring data

We now illustrate the findings from the previous sections with detailed emission data from the Institute for Radio-Elements (IRE) located in Fleurus, Belgium. The emission data have the highest available temporal resolution of 15 min for a full year, 2014. ^{133}Xe releases can

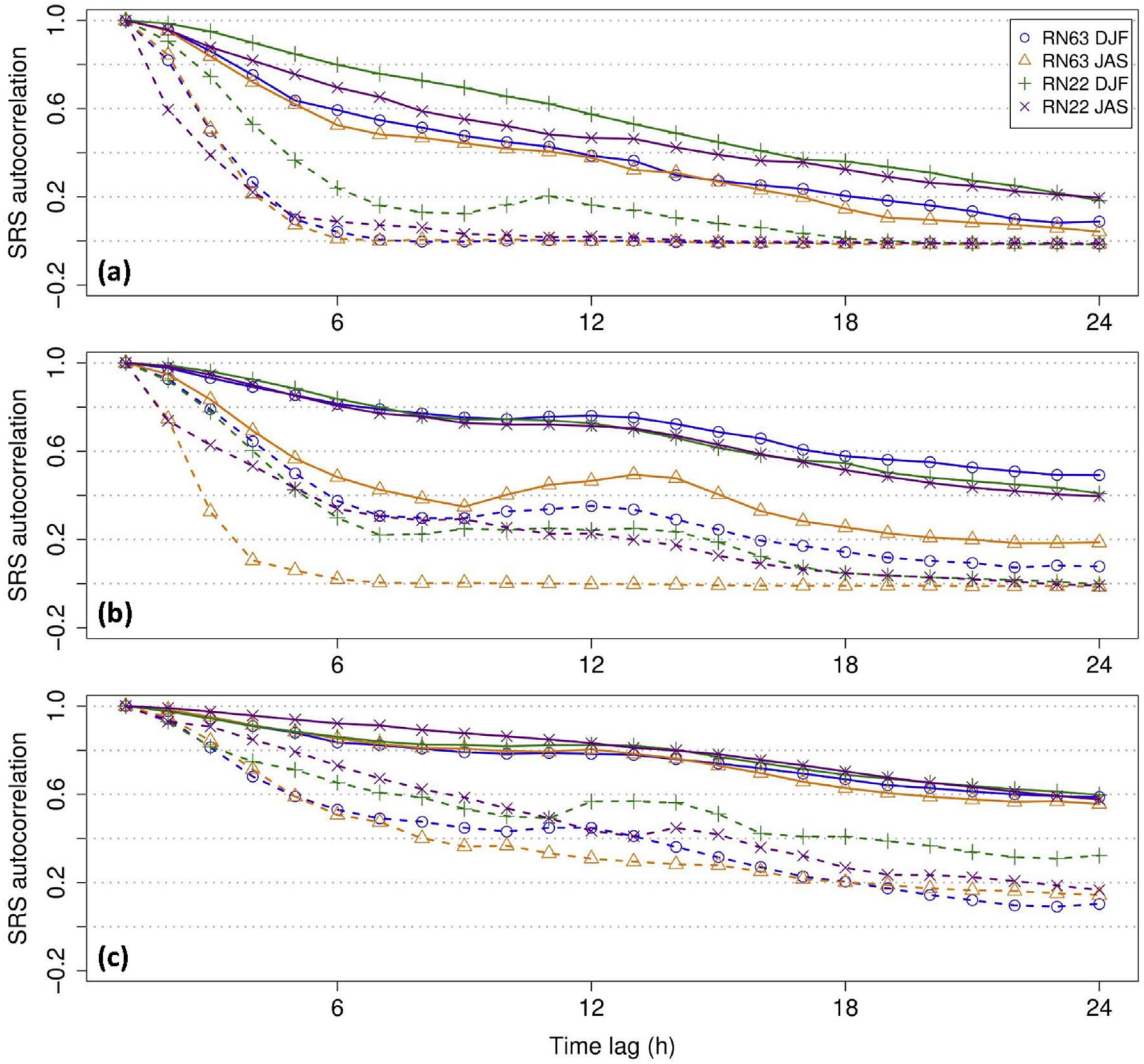

Fig. 3. Median (solid lines) and 0.05 quantile (dashed lines) of the source-receptor-sensitivity autocorrelation as a function of the time lag for a source-receptor distance of approx. (a) 300 km, (b) 1000 km and (c) 5000 km. Results are given for the two IMS stations and the two periods considered in this study.

vary by many orders of magnitude during only a few hours, while remaining fairly constant during the rest of the day. A description of the stack monitoring system at IRE can be found in Deconninck and De Lellis (2013).

A new set of Flexpart runs have been performed in forward mode. Each individual simulation covered the year 2014 (this year has been chosen due to the availability of IRE emission data). The simulations differed by their emission data: a control simulation used the 15 min ^{133}Xe emission data, while the other simulations used time-averaged emissions, yielding 3-hourly, daily or constant ^{133}Xe releases. Since we are interested in the error resulting from the temporal resolution of the emission data, the control simulation, using emission data with the highest available temporal resolution, can be seen as the "truth". In the paragraphs below, "error" thus refers to the difference between the simulation with time-averaged emission data and the control simulation with the most accurate emission data. The Flexpart model setup and the driving meteorological data are the same as described in section 2, except for the differences outlined above. The Flexpart output for January 2014 has been omitted in the analyses, to ensure spin-up over the full domain.

As an example, the absolute error (AE) of the activity concentration for different emission data is shown in Fig. 6, for a single day assuming a 24 h sampling period (that is, the activity concentrations were simply averaged during 24 h). The absolute error of a quantity x is defined as the absolute difference between its true value x_{true} and its simulated value x_{sim}:

$$AE = |x_{true} - x_{sim}| \quad (5)$$

In Fig. 6, it can be seen that the absolute error consists of a few spots which are strongly confined in space and time. These spots correspond to short peak releases at IRE and are transported and diluted with time. As such plumes move further, the activity concentration decreases due to decay and atmospheric dispersion. The corresponding error consequently also decreases with time. From Fig. 6, it is clear that the absolute error decreases when using better time-resolved emission data.

We are now interested in the mean absolute error resulting from poorly time-resolved emission data for the period February–December 2014 (Fig. 7a–c). A key feature, in agreement with the conclusions from section 3, is that the error originating from emission data with coarse temporal resolution is negligible in a large part of the domain, except nearby the source. This is not surprising since the errors are confined in space and time (Fig. 6), and furthermore decrease due to decay, dilution and the smoothing of the SRS dependency with time. The latter is further illustrated by the mean relative error (RE) for the period February–December 2014 (Fig. 7d–f). For that, only data pairs where the control simulation had activity concentrations above 0.1 mBq/m^3 were used in order to avoid very large relative errors from the division of very small numbers:

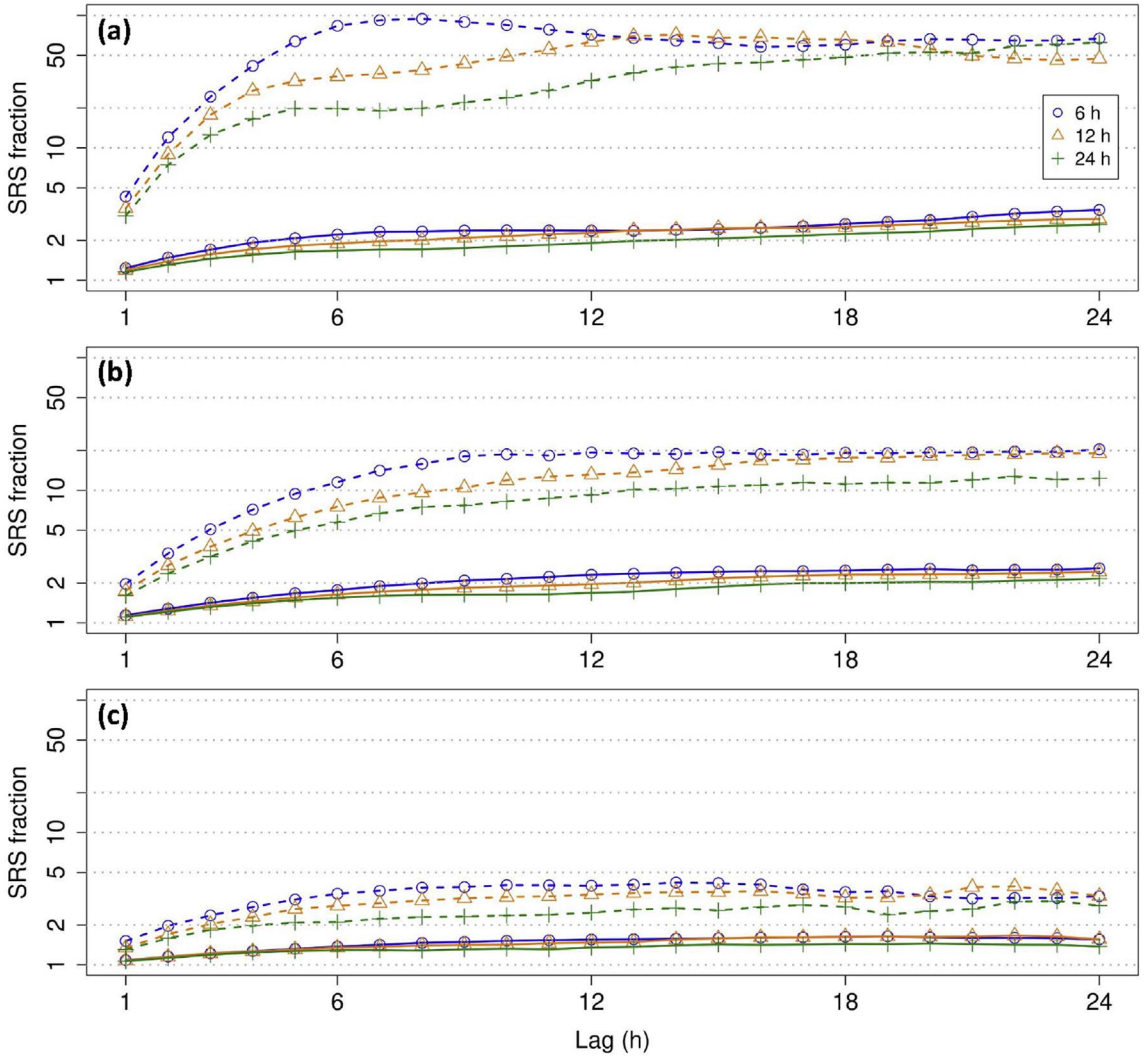

Fig. 4. Median (solid lines) and 0.95 quantile (dashed lines) of the fractions of source-receptor-sensitivity pairs separated by a certain time lag for a source-receptor distance of approx. (a) 300 km, (b) 1000 km and (c) 5000 km. The larger SRS value is always divided by the smaller, so that no values are smaller than 1. Results are given for a sampling time of 6 h, 12 h and 24 h.

$$RE = \frac{|x_{true} - x_{sim}|}{x_{true}} \text{ for } x_{true} > 0.1 \text{ mBq/m}^3 \quad (6)$$

We conclude that generally a constant emission could be sufficient for atmospheric transport and dispersion modelling problems on the synoptic scale. In order to reduce the error close to the source, time-resolved emission data are needed (Fig. 7). Similar plots like Fig. 7 have been generated for the smaller sampling periods 12 h and 6 h, but there was hardly any noticeable effect (not shown).

Although the mean absolute error shows that on average time-resolved emission data are only relevant nearby the source (Fig. 7), it should also be investigated what the maximum absolute error can be at a certain location, as suggested by the 0.95 quantile in Fig. 2 and the 0.05 quantile in Fig. 3. For that purpose, the maximum absolute error at each grid box is plotted in Fig. 8. It can be seen that a significant part of the northern hemisphere can have errors large enough to affect the IMS noble gas stations. The use of time-resolved emission data decreases the maximum absolute error. The effect of reducing the sampling time from 24 h to 6 h is also shown in Fig. 8: a smaller sampling time (Fig. 8b, d, f) increases the maximum error originating from poorly time-resolved emission data. With 6 h sampling and daily resolved emission data (Fig. 8d), the maximum absolute error is larger than the maximum absolute error for a constant release with 24 h sampling time (Fig. 8a).

6. Effect of horizontal resolution

The backward Flexpart simulations for station RN63, period DJF, have been repeated on a smaller domain with horizontal grid spacings of 0.25° instead of 1°. The meteorological data were as described in section 2, but with horizontal grid spacings of 0.25°. The aim is to check whether our conclusions made above for the source-receptor distances of approximately 300 km are still valid at higher spatial resolutions. The simulation length has been reduced to 14 days, which is sufficient for the smaller domain. For consistency, the simulation length of the runs with 1° horizontal grid spacings have been reduced to 14 days in this analysis. The same fictitious sources shown in Fig. 1a have been used, since the air masses have roughly identical origins. For the experiments at 0.25° grid spacings, the SRS threshold has been decreased by a factor of 16, since the grid box volume is lower by the same factor.

Fig. 9a shows the SRS fractions for the source-receptor distance of 300 km for the simulations with 1° and 0.25° horizontal grid spacings. The median SRS fractions are almost identical. The 0.95 quantile for the simulation at 0.25° grid spacings is twice as large for the shorter time lags, but is slightly smaller at later time lags. The former is likely due to the fact that, at higher spatial resolution, small-scale atmospheric features are better resolved, which typically occur on short time scales. As a further check, we have included results for the station at approx.

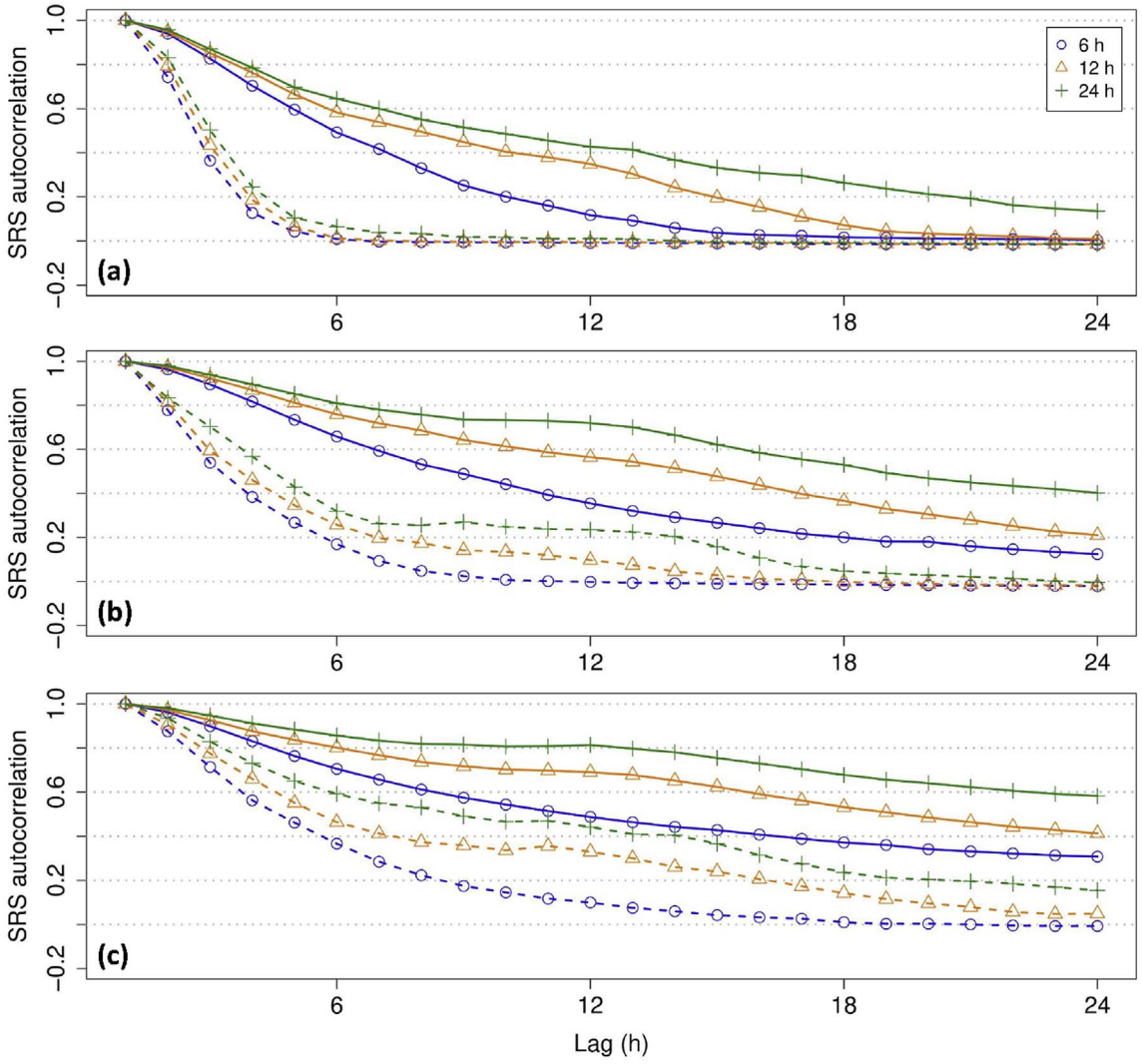

Fig. 5. Median (solid lines) and 0.05 quantile (dashed lines) of the source-receptor-sensitivity autocorrelation as a function of the time lag for a source-receptor distance of approx. (a) 300 km, (b) 1000 km and (c) 5000 km. Results are given for a sampling time of 6 h, 12 h and 24 h.

1000 km (Fig. 9b). The SRS fractions are very similar for both sets of simulations.

The new simulations were run with the same number of particles as for the previous simulations (instead of increasing the number of particles, the domain and simulation length have been decreased), so that the average number of particles per grid box is different. SRS values below the SRS threshold are therefore better resolved in the simulations with 1° grid spacings, so that a comparison of the autocorrelation is not possible.

Finally, we test our findings with real stack emission data from IRE as in section 5. We have repeated the forward Flexpart simulations with 0.25 horizontal grid spacings on a smaller domain for the period Jan–Mar 2014 (we have not repeated the simulations for a full year due to the computational costs). The mean absolute error is shown in Fig. 10. The results are similar to those shown in Fig. 7 (top), though the errors are less smoothed since the simulations covered a shorter period.

7. Discussion and conclusions

Radioxenon (^{131m}Xe, ^{133m}Xe, ^{133}Xe and ^{133}Xe) emissions from

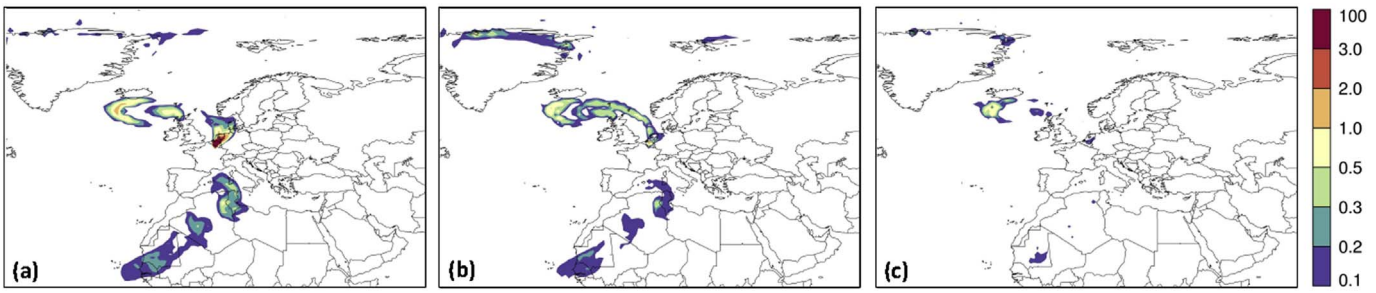

Fig. 6. Absolute error of the activity concentration (mBq/m^3) for 1 February 2014 with a 24 h sampling period for different emission data: (a) constant release (mean release for 2014), (b) constant release (mean release for 1 February 2014) and (c) 3-hourly release.

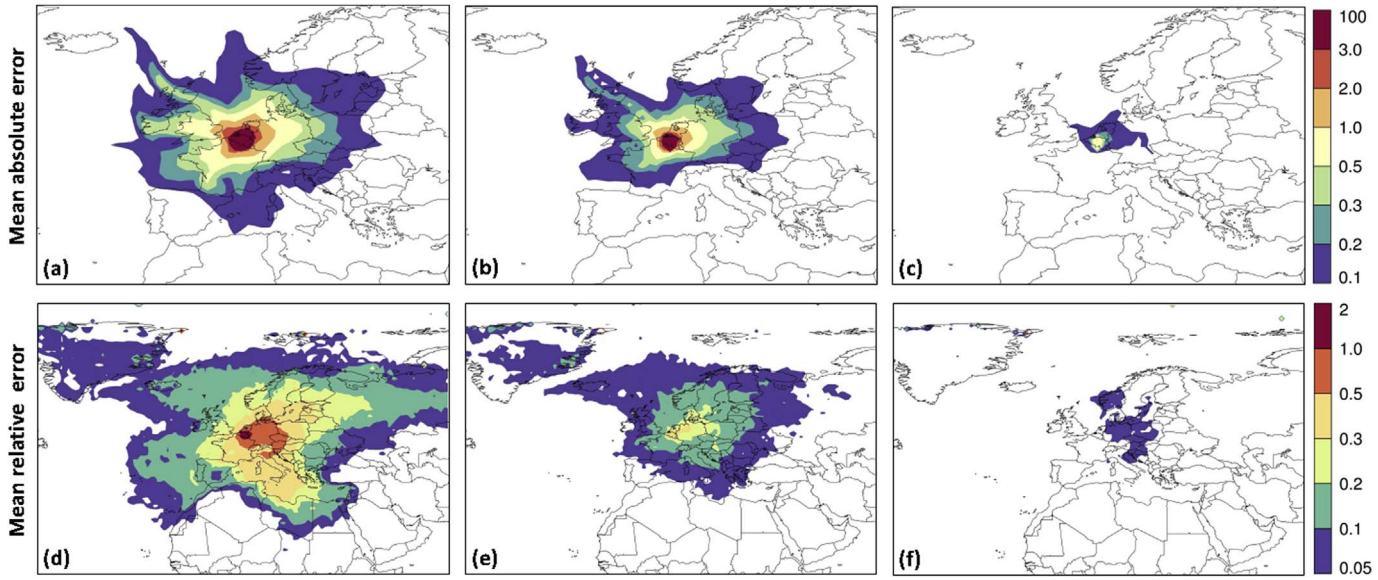

Fig. 7. Top row: mean absolute error of the activity concentration (mBq/m^3) assuming 24 h sampling for different emission data: (a) constant release, (b) daily release and (c) 3 h release. Bottom row: mean relative error of the activity concentration assuming 24 h sampling for different emission data: (d) constant release, (e) daily release and (f) 3 h release. Note that the domains are slightly different for top and bottom rows.

civilian sources deteriorate the capability of the International Monitoring System to verify compliance with the Comprehensive Nuclear-Test-Ban Treaty. Therefore, understanding the radioxenon background is important and has been addressed in several studies. At IMS noble gas stations, the radioxenon background can vary significantly from day to day, so that explicitly modelling the contribution from civilian sources might be necessary to discriminate the signatures of civilian sources from those of nuclear explosions. However, this is a challenging task since it involves many uncertainties and requires significant computational resources. Furthermore, stack emission data from the civilian sources are currently not available for simulating the daily radioxenon background in an operational context, at least partly because of the commercial value of such data. However, awareness is being created on the impact on the noble gas component of the verification regime of the Comprehensive Nuclear-Test-Ban Treaty and emission data could become available in the future for explicitly modelling the daily radioxenon background in an operational context.

In this paper, we have assessed which temporal resolution emission data should ideally have in order to better simulate the civilian background in an operational context. For that, we have run the Lagrangian particle dispersion model Flexpart in backward mode and have assessed the temporal variation of the source-receptor-sensitivities (SRS) for fixed locations at distances of approximately 300, 1000 and 5000 km. This methodology has the advantage that it is independent of the emission data but instead focusses on how well the atmospheric transport model itself can “digest ” the time-dependency of the emission data.

It was found that significant SRS values generally do not vary much within 24 h, especially for source-receptor distances of 1000 km and more, corresponding to atmospheric transport and dispersion problems on the synoptic scale (Fig. 2). However, for specific meteorological conditions, the SRS values can change significantly within only a few hours. This shows that daily emission data should be sufficient for most cases, although sometimes emission data with a higher temporal resolution are necessary. These cases can be identified by the atmospheric transport and dispersion model itself. For source-receptor distances of a few hundred kilometres, the SRS values can vary two orders of magnitude within 24 h. Time-resolved emission data are thus important

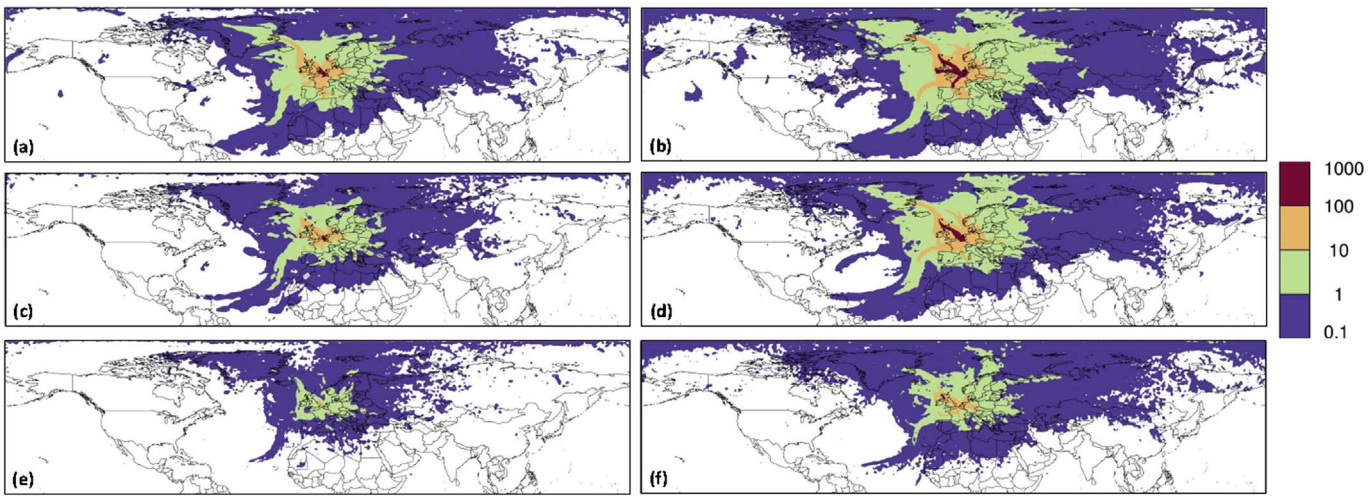

Fig. 8. Maximum absolute error of the activity concentration (mBq/m^3) at each grid box for different emission data and sampling times; (a) yearly release, 24 h sampling; (b) yearly release, 6 h sampling; (c) daily release, 24 h sampling; (d) daily release, 6 h sampling; (e) 3-hourly release, 24 h sampling and (f) 3-hourly release, 6 h sampling.

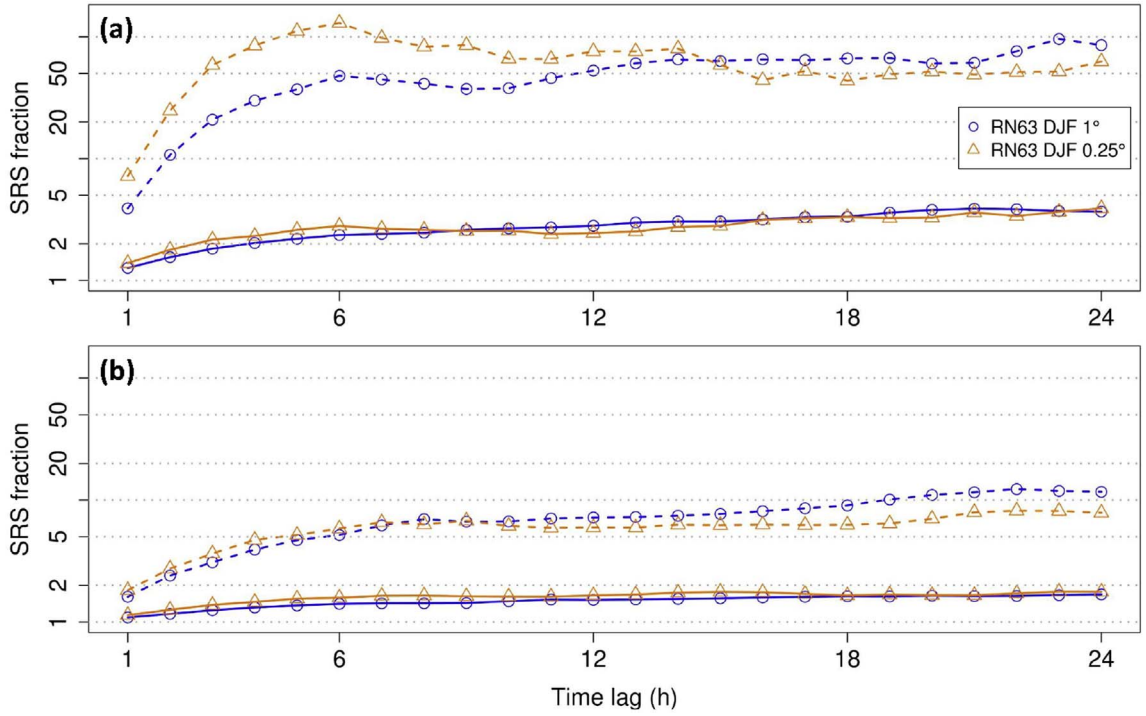

Fig. 9. Median (solid lines) and 0.95 quantile (dashed lines) of the fractions of source-receptor-sensitivity pairs separated by a certain time lag for a source-receptor distance of approx. (a) 300 km and (b) 1000 km. The larger SRS value is always divided by the smaller, so that no values are smaller than 1. Results are given for simulations at 1° and 0.25° horizontal grid spacings.

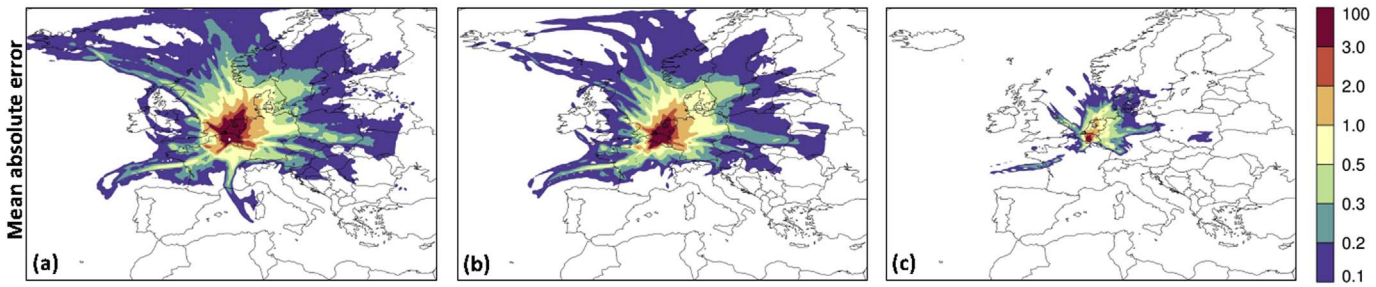

Fig. 10. Mean absolute error of the activity concentration (mBq/m^3) assuming 24 h sampling for different emission data: (a) constant release for 2014, (b) daily release and (c) 3 h release.

when the source-receptor distance is less than a few hundred kilometres. Similar conclusions were found based on the SRS autocorrelation (Fig. 3) and with simulations at smaller horizontal grid spacings (Fig. 9).

There are more nuclear power plants than medical isotope production facilities, and thus, more nuclear power plants are close to an IMS station. These nuclear power plants typically emit far less radioxenon than the medical isotope production facilities, so that they do not affect the IMS noble gas stations as much. However, for short source-receptor distances, the need to have time-resolved emission data might be important for nuclear power plants. This could be assessed further with simulations at higher spatial resolutions and by varying the SRS threshold.

Shorter sampling periods have the potential to allow a better source reconstruction as it results in more data being available for the inverse atmospheric transport modelling. However, at the same time, it increases the need for time-resolved emission data, since shorter sampling periods lead to an increase in the SRS variability (Fig. 4) and a decrease in the SRS autocorrelation (Fig. 5).

The above findings have been illustrated by using emission data from the Institute for Radio-Elements for the year 2014. The mean absolute error originating from poorly time-resolved emission data is negligible at large source-receptor distances, but significant close to the source (Fig. 7). This is in agreement with Schöppner et al. (2013), who found that daily emission data improved results over emission data with coarser temporal resolution for an IMS station at 700 km from the source, but had no impact for an IMS station at 3000 km from the source. In order to reduce the mean absolute error nearby the source, time-resolved emission data are required. In specific meteorological conditions, the error from poorly time-resolved emission data can be significant over a large part of the Northern Hemisphere (Fig. 8). A smaller sampling time increases the maximum error that can originate from poorly time-resolved emission data (Fig. 8).

From the findings above, time-resolved emission data are generally not needed to simulate the day-to-day ^{133}Xe background at IMS stations. However: (i) for sources within a few hundred kilometres from an IMS station, time-resolved emission data is desirable and (ii) in case of specific meteorological conditions, a significant event or a significant mismatch between simulation and observation, it is desirable to have available emission data with the highest temporal resolution. In practice, the required temporal resolution should be chosen by considering Figs. 2 and 3, but also by considering which error coming from emission data is thought to be acceptable, and (if possible) by considering the temporal variability of the emission data.

Simulations with horizontal grid spacings of 0.25° suggest that the findings above are also valid at higher resolutions (Figs. 9 and 10).

Only simulations for ^{133}Xe have been presented, but conclusions are likely similar for ^{131m}Xe and ^{133m}Xe. For ^{135}Xe, a larger error could occur from averaged emission data due to the shorter half-life, since one cannot differentiate between a strong release at the beginning of the release period or a weak release at the end of the release period.

Lastly, the results are also relevant for inverse modelling, as they show that models are generally not able to resolve sharp temporal variations in the release term for long-range transport and dispersion problems.

Acknowledgments

The first author acknowledges funding from Engie under contract number JUR2015-28-00. The authors would like to thank the three anonymous reviewers for their helpful comments.

Appendix A. Supplementary data

Supplementary data related to this article can be found at http://dx.doi.org/10.1016/j.jenvrad.2017.11.027.

References

Achim, P., Generoso, S., Morin, M., Gross, P., Le Petit, G., Moulin, C., 2016. Characterization of Xe-133 global atmospheric background: implications for the international monitoring system of the comprehensive nuclear-test-ban treaty. J. Geophys. Res. Atmos. 121, 4951–4966.

Appelhans, A.D., Turnbull, J.A., 1981. Measured Release of Radioactive Xenon, Krypton, and Iodine from UO2 at Typical Light Water Reactor Conditions, and Comparison with Release Models. The Commission.

Chang, C.P., 2004. East Asian Monsoon, vol. 2 World Scientific.

De Meutter, P., Camps, J., Delcloo, A., Deconninck, B., Termonia, P., 2016. On the capability to model the background and its uncertainty of CTBT-relevant radioxenon isotopes in Europe by using ensemble dispersion modeling. J. Environ. Radioact. 164, 280–290.

Deconninck, B., De Lellis, C., 2013. High resolution monitoring system for IRE stack releases. J. Environ. Radioact. 125, 61–68. http://dx.doi.org/10.1016/j.jenvrad.2013.01.016.

Draxler, R.R., Rolph, G.D., 2012. Evaluation of the Transfer Coefficient Matrix (TCM) approach to model the atmospheric radionuclide air concentrations from Fukushima. J. Geophys. Res. Atmos. 117.

Emanuel, K.A., Živković-Rothman, M., 1999. Development and evaluation of a convection scheme for use in climate models. J. Atmos. Sci. 56, 1766–1782.

Eslinger, P.W., Bowyer, T.W., Achim, P., Chai, T., Deconninck, B., Freeman, K., Generoso, S., Hayes, P., Heidmann, V., Hoffman, I., et al., 2016. International challenge to predict the impact of radioxenon releases from medical isotope production on a Comprehensive Nuclear-Test-Ban Treaty sampling station. J. Environ. Radioact. 157, 41–51. http://dx.doi.org/10.1016/j.jenvrad.2016.03.001.

Fontaine, J.P., Pointurier, F., Blanchard, X., Taffary, T., 2004. Atmospheric xenon radioactive isotope monitoring. J. Environ. Radioact. 72, 129–135. http://dx.doi.org/10.1016/S0265-931X(03)00194-2.

Gueibe, C., Kalinowski, M.B., Baré, J., Gheddou, A., Krysta, M., Kusmierczyk-Michulec, J., 2017. Setting the baseline for estimated background observations at IMS systems of four radioxenon isotopes in 2014. J. Environ. Radioact. 178, 297–314.

Hanna, S.R., Briggs, G.A., Hosker Jr., R.P., 1982. Handbook on Atmospheric Diffusion. Technical Report. National Oceanic and Atmospheric Administration, Oak Ridge, TN (USA). Atmospheric Turbulence and Diffusion Lab.

Hayes, J.C., Ely, J.H., Haas, D.A., Harper, W.W., Heimbigner, T.R., Hubbard, C.W., Humble, P.H., Madison, J.C., Morris, S.J., Panisko, M.E., et al., 2015. Requirements for Xenon International. Technical Report. Pacific Northwest National Laboratory (PNNL), Richland, WA (US). http://dx.doi.org/10.2172/1122330.

Hoffman, I., Ungar, K., Bean, M., Yi, J., Servranckx, R., Zaganescu, C., Ek, N., Blanchard, X., Le Petit, G., Brachet, G., et al., 2009. Changes in radioxenon observations in Canada and Europe during medical isotope production facility shut down in 2008. J. Radioanalytical Nucl. Chem. 282, 767.

Kalinowski, M.B., Grosch, M., Hebel, S., 2014. Global Xenon-133 emission inventory caused by medical isotope production and derived from the worldwide Technetium-99m demand. Pure Appl. Geophys. 171, 707–716. http://dx.doi.org/10.1007/s00024-013-0687-5.

Kalinowski, M.B., Pistner, C., 2006. Isotopic signature of atmospheric xenon released from light water reactors. J. Environ. Radioact. 88, 215–235.

Matthews, K., Bowyer, T., Saey, P., Payne, R., 2012. The workshop on signatures of medical and industrial isotope production–WOSMIP; Strassoldo, Italy, 1–3 july 2009. J. Environ. Radioact. 110, 1–6.

Maurer, C., Eslinger, P., Bar, J., Kusmierczyk-Michulec, J., Seibert, P., Orr, B., Philipp, A., Ross, O., Generoso, S., Achim, P., Schoeppner, M., Malo, A., Ringbom, A., Saunier, O., Quelo, D., Mathieu, A., Kijima, Y., Crawford, A., Stein, A., Chai, T., Ngan, F., Leadbetter, S., De Meutter, P., Delcloo, A., Britton, R., Davies, A., Glascoe, L., Lucas, D., Simpson, M., Vogt, P., Kalinowski, M., Bowyer, T., 2017. International challenge to model the long-range transport of radioxenon released from medical isotope production to six Comprehensive Nuclear-Test-Ban Treaty monitoring stations. Submitt. J. Environ. Radioact.

Panagiotopoulos, F., Shahgedanova, M., Hannachi, A., Stephenson, D.B., 2005. Observed trends and teleconnections of the Siberian high: a recently declining center of action. J. Clim. 18, 1411–1422.

Ringbom, A., Aldener, M., Axelsson, A., Fritioff, T., Kastlander, J., Mörtsell, A., Olsson, H., 2017. In: The SAUNA III Project, Presented at the CTBT: Science and Technology Conference, Vienna, 2017.

Ringbom, A., Larson, T., Axelsson, A., Elmgren, K., Johansson, C., 2003. SAUNA: a system for automatic sampling, processing, and analysis of radioactive xenon. Nuclear Instruments and Methods in Physics Research Section A: accelerators, Spectrometers. Detect. Assoc. Equip. 508, 542–553. http://dx.doi.org/10.1016/S0168-9002(03)01657-7.

Saey, P.R., 2009. The influence of radiopharmaceutical isotope production on the global radioxenon background. J. Environ. Radioact. 100, 396–406. http://dx.doi.org/10.1016/j.jenvrad.2009.01.004.

Schöppner, M., Kalinowski, M., Plastino, W., Budano, A., de Vincenzi, M., Ringbom, A., Ruggieri, F., Schlosser, C., 2014. Impact of monthly radioxenon source time-resolution on atmospheric concentration predictions. Pure Appl. Geophys. 171, 699–705.

Schöppner, M., Plastino, W., Hermanspahn, N., Hoffmann, E., Kalinowski, M., Orr, B., Tinker, R., 2013. Atmospheric transport modelling of time resolved 133Xe emissions from the isotope production facility ANSTO, Australia. J. Environ. Radioact. 126, 1–7. http://dx.doi.org/10.1016/j.jenvrad.2013.07.003.

Seibert, P., Frank, A., 2004. Source-receptor matrix calculation with a Lagrangian particle dispersion model in backward mode. Atmos. Chem. Phys. 4, 51–63.

Seibert, P., Krüger, B., Frank, A., 2001. Parametrisation of convective mixing in a Lagrangian particle dispersion model. In: Proceedings of the 5th GLOREAM Workshop, pp. 24–26 Wengen, Switzerland.

Stohl, A., Forster, C., Frank, A., Seibert, P., Wotawa, G., 2005. Technical note: the lagrangian particle dispersion model FLEXPART version 6.2. Atmos. Chem. Phys. 5, 2461–2474. http://dx.doi.org/10.5194/acp-5-2461-2005.

Stohl, A., Hittenberger, M., Wotawa, G., 1998. Validation of the Lagrangian particle dispersion model FLEXPART against large-scale tracer experiment data. Atmos. Environ. 32, 4245–4264. http://dx.doi.org/10.1016/S1352-2310(98)00184-8.

Stohl, A., Thomson, D.J., 1999. A density correction for Lagrangian particle dispersion models. Boundary-Layer Meteorol. 90, 155–167. http://dx.doi.org/10.1023/A:1001741110696.

Topin, S., Le Petit, G., Piwowarczyk, J., Philippe, T., Cagniant, A., Delaune, O., Gross, P., Douysset, G., Moulin, C., 2017. SPALAX-new generation: deployment, operation and performances. In: Presented at the CTBT: Science and Technology Conference, Vienna, 2017.

Vogelezang, D.H., Holtslag, A.A., 1996. Evaluation and model impacts of alternative boundary-layer height formulations. Boundary-Layer Meteorol. 81, 245–269.

WOSMIP, 2016. In: Workshop on Signatures of Man-made Isotope Production, . http://wosmip.pnnl.gov/, Accessed date: 21 August 2017.

Wotawa, G., Becker, A., Kalinowski, M., Saey, P., Tuma, M., Zähringer, M., 2010. Computation and analysis of the global distribution of the radioxenon isotope 133Xe based on emissions from nuclear power plants and radioisotope production facilities and its relevance for the verification of the Nuclear-Test-Ban Treaty. Pure Appl. Geophys. 167, 541–557. http://dx.doi.org/10.1007/s00024-009-0033-0.

Wu, B., Wang, J., 2002. Winter arctic oscillation, Siberian high and East asian winter monsoon. Geophys. Res. Lett. 29.